

Remote Quantification of Total Suspended Matter through Empirical Approaches for Inland Waters

K. S. Song^{1,2,*}, L. Li², L. Tedesco³, H. T. Duan⁴, L. H. Li², and J. Du¹

¹Northeast Institute of Geography and Agricultural Ecology, CAS, Changchun 130102, China

²Department of Earth Sciences, Indiana University-Purdue University, Indianapolis, IN 46202, USA

³The Wetlands Institute, Stone Harbor, NJ 08247, USA

⁴Nanjing Institute of Geography and Limnology, CAS, Nanjing 210008, China

Received 13 July 2012; revised 22 April 2013; accepted 5 September 2013; published online 21 March 2014

ABSTRACT. The present study is focused on remote quantification of total suspended matter (TSM) for turbid inland waters. In situ remote sensing reflectance (Rrs) and TSM at 863 stations over 10 inland water bodies from China, Australia, and USA were collected and examined. Four empirical regression models based on sensitive reflectance bands (SB), derivatives (SD), the band ratio proposed by Doxaran et al. (2002; Rrs850/Rrs550: DM), and optimal band ratios (OBR) were examined to estimate TSM. The performance varies due to TSM concentration and the Chl-a: TSM ratio. The four models perform well when the water bodies are dominated with non-algal particles at high TSM concentration and yielded higher accuracy (R^2 ranged from 0.83 to 0.91) with both DM and OBR models, while the OBR model outperformed other models when waters are dominated by phytoplankton. Our findings also indicate that phytoplankton in the water column affects the band ratio algorithm for TSM estimates. When data from all water bodies are considered collectively, the OBR model ($R^2 = 0.92$) marginally outperforms the other three models (0.89, 0.87, and 0.88 for DM, SB, and SD, respectively). Future studies should be undertaken to analyze the influence of phytoplankton abundance on water-leaving signals for TSM estimates. The results of the present study also need further analyses to gain a more in-depth understanding of inherent optical properties for optically active constituents (OACs), such as absorption and backscattering to interpret the observed variations.

Keywords: absorption, chlorophyll, hyperspectral, total suspended matter

1. Introduction

Total suspended matter (TSM) has a critical impact on light propagation in the water column. For inland waters, TSM is often related to nitrogen, phosphorus, heavy metal and micropollutant fluxes (Dekker et al., 2002; Hu et al., 2004). In many turbid regions, TSM is directly related to sediment transportation (Fettweis et al., 2006), and to the availability of light for primary production (Doxaran et al., 2002; Hu et al., 2004). The concentrations and budgets are strongly influenced by sedimentation and soil erosion via river discharge. As such, TSM relates to the environment, ecology, fishery, and economy of inland waters (Panigrahi et al., 2009). Given that TSM is spatially heterogeneous, a synoptic view of TSM concentration is very difficult to obtain by merely using an *in situ* monitoring network (Song et al., 2012), and an optimal mapping approach is a combination of remote sensing, *in situ* measurements, and water quality modeling (Stumpf and Pennock, 1989; Han and Rundquist, 1997; Doxaran et al., 2002). De-

monstrating strong spectral signals, TSM can be evidently mapped from the top-of-atmosphere radiance (Stumpf and Pennock, 1989; Hu et al., 2004; Odermatt et al., 2012) or with photographs taken from space (Acker et al., 2005). Algorithms for remote estimation of TSM in oceanic and coastal waters are well developed, however, improving the performance of these algorithms for monitoring inland waters is still required for spatially and compositionally heterogeneous patterns caused by soil erosion and other anthropogenic impacts (Dekker et al., 2002; Doxaran et al., 2006; Song et al., 2012).

In nature, the upwelling radiance from waters is an integration of spectral signal from all constituents in a water column. In a shallow aquatic system, the bottom may also contribute to the amount of water-leaving radiance (Gons, 1999; Ma et al. 2006). The influence of TSM or suspended minerals on chlorophyll-a (Chl-a) inversion has been widely recognized (Gons, 1999; Gitelson et al., 2008; Yang et al., 2011). Chen et al. (1992) reported that the first derivative of remote sensing reflectance can be used to reduce water-sediment composite signals, and the presence of significant and spectrally variable environmental effects can be partially removed or reduced through derivative transformation. Derivative analysis has proven effective in reducing the effect of TSM on Chl-a estimation in controlled experiments with va-

* Corresponding author. Tel.: +86 431 85542364; fax: +86 431 85542298.

E-mail address: jujiewang@126.com (K. S. Song).

rying suspended-sediment concentrations for the spectral domain between 400 and 900 nm (Han et al., 1994; Rundquist et al., 1996; Sváb et al., 2005). In contrast, few investigations have been conducted to explore the influence of phytoplankton abundance on TSM estimates (Acker et al., 2005).

Band ratio algorithms are widely used to determine TSM concentration using remote sensing data acquired from various platforms (Doxaran et al., 2002; Myint and Waker, 2002; Hu et al., 2004; Sváb et al., 2005; Petus et al., 2010; Song et al., 2012) for coastal and inland waters. The differences in accuracy for the TSM estimation are due to the independent variability of optically active constituents (OACs) in case-II waters (Nechad et al., 2010). The band ratios used in these studies are based on the properties of the near-infrared (NIR) reflectance increasing with high concentration of inorganic particles (Doxaran et al., 2002), or the ratio of the reflectance peak to the reflectance at 550 nm. On the basis of the conceptual bio-optical model (Gordon et al., 1975), Doxaran et al. (2002, 2003, and 2005) proved that the band ratio algorithm is effective in reducing the effects caused by sediment composition and grain-size, in addition to illumination conditions.

Semi-empirical algorithms are also based on the bio-optical model through linking remote sensing reflectance (Rrs) to water inherent optical properties (IOPs), that is, bulk absorption (a) and backscattering (b_b): $R = f \cdot (b_b/a + b_b)$, where R is the irradiance reflectance just beneath the water surface (Gordon et al., 1975). Algorithms based on bio-optical models have shown a promise to be spatiotemporally transferable (Stumpf and Pennock, 1989; Dekker et al., 2001; Nechad et al., 2010). The use of bio-optical models for simultaneously estimating inorganic suspended matter (ISM), Chl-*a*, and colored dissolved organic matter (CDOM) has been extensively documented by Brando and Dekker (2003) who presented the application of bio-optical models for the assessment of coastal water quality. In addition, Hans et al. (2002) demonstrated the successful application of the models for monitoring inland waters. However, few studies have assessed the effects of TSM type (silt, clay, or other types, as well as grain size and refractive index) and composition (algal vs. non-algal proportion) on the spectral signatures of inland waters (Doxaran et al., 2003; Binding et al., 2005). Therefore, the spatial and temporal transferability of bio-optical models in quantifying TSM is still uncertain.

Benefiting from bio-optical modeling and deep insights into the IOPs, some empirical models have evolved into semi-empirical models (Forget et al., 1999; Babin et al., 2003; Acker et al., 2005). Both empirical and semiempirical model forms have been selected on the basis of simplified optical models and assumptions (Doxaran et al., 2002, 2003). The objectives of the present paper are to examine the spectral reflectance of inland waters characterized by heterogeneous TSM and Chl-*a* concentrations, and identify an appropriate empirical approach that could aid the quantification of TSM in the presence of variable Chl-*a* concentrations. The outline of the present paper is as follows: First, data collection and pre-processing methods are described. Second, two essential

processing steps, i.e. spectral data processing and the algorithm that relates the Rrs to TSM concentration, are developed. These aspects are reflected in the empirical model results for various datasets with diverse TSM concentrations with optimal band ratio algorithm (OBR), Doxaran et al. (2002) model (DM), the most sensitive spectral band (SB) and sensitive derivative reflectance (SD) models for TSM estimation.

2. Materials and Methods

2.1. Study Sites

Data sets from 10 water bodies from three countries were used to test or establish various empirical methods for TSM estimates with *in situ* collected spectra. Two spectrometers and three spectroradiometric measurement protocols were applied during the various field surveys.

2.1.1. Northeast and East China Sites

The Shitoukoumen Reservoir (STKR: 43°52'58.75" N, 125°48'58.49" E; area (A) = 42.0 km²; depth (Z) = 6.3 m) and Songhua Lake (SHL: 43°38'41.57" N, 26°47'53.85" E; A = 550.0 km²; Z = 35.0 m) are the major drinking and recreational water systems for over 5.1 million residents of Jilin province, China. The Shitoukoumen Reservoir is impaired by soil erosion and agricultural non-point pollution (Xu et al., 2009). The catchment up to the dam of Songhua Lake is mainly composed of forest (72%), and major pollutants also come from agricultural and residential sources through some tributaries. Twelve/six field surveys on the STKR/SHL were conducted during 2006-2008, where 178 and 156 samples were collected, respectively.

Lake Chagan (CGL: 45°14'33.52" N, 124°17'49.48" E; A = 372.0 km²; Z = 1.52 m), is located in the Southwest of Songnen Plain. Water from the Songhua River is discharged into the CGL bringing large amounts of suspended sediments. In addition, resuspension from the lake bottom contributes to TSM because of shallow lake depths coupled with strong winds. CGL is also a eutrophic lake with high Chl-*a* concentration, and low clarity (Song et al., 2011). There were 99 samples collected from 2009 to 2010.

Taihu Lake (THL: 31°10'45.24" N, 120°10'27.21" E; A = 2338.1 km²; Z = 1.9 m) is the largest fresh water body in East China with an average storage capacity of 4.76×10^{10} m³. As a typical shallow inland lake, THL is a large eutrophic water system with high spatial heterogeneity (Ma et al., 2006). Various aquatic ecosystems are distributed over the lake, such as algal-dominated, macrophyte-dominated, and transition zones, with complicated seasonal dynamics of phytoplankton, inorganic particulate matter, and CDOM. Altogether, 94 samples were collected in October 2008 and May 2010.

2.1.2. South Australia Sites (SA)

The Myponga Reservoir (MPR) is an inland potable water source (35°24'10.02" S, 138°26'13.29" E; A = 2.8 km²;

$Z = 21.5$ m), located about 60 km south of Adelaide, and providing approximately 5% of the drinking water for the city. The Murray River at Mannum (MRM) is situated on the broad reaches of the Lower Murray River (34°44'55.11" S, 139°19'33.22" E; $Z = 5.6$ m), and one of the main pumping stations supplying water to Adelaide is situated in this area. The Murray River at Wellington (MRW) is connected to Alexandrina Lake (35°23'55.19" S, 139°27'33.11" E; $Z = 5.3$ m) just upstream of where it empties into the Lake. The river is adjacent to the coast of the Southern Ocean, serving as major drinking-water source for Adelaide through pumping stations. Six field surveys were conducted over the three potable waters from February to March 2009 yielding a total of 60 samples (see Table 1).

2.1.3. Central Indian Sites (CIN)

Eagle Creek (ECR: 39°51'09.84" N, 86°18'13.07" W; $A = 5.0$ km²; $Z = 4.2$ m), Morse (MR: 40°6'16.84" N, 86°2'17.22" W; $A = 6.0$ km²; $Z = 4.7$ m), and Geist Reservoirs (GR: 35°56'16.84" N, 85°57'47.22" W; $A = 7.5$ km²; $Z = 3.2$ m) are the major drinking water systems supplying potable water for over 900,000 residents in the Indianapolis Metropolitan region, Indiana. Seventeen field surveys were conducted under widely diverse sun angles and sky conditions in 2005 and 2006 and resulted in 276 samples.

2.2. In Situ Data Collection

Samples were obtained under a diverse range of suspended matter and algal bloom conditions (TSM and Chl-*a* concentrations ranging from 1.69 to 413.9 mg/L and 2.69 to 183.2 µg/L, respectively). *In situ* water measurements were collected using an YSI 600 XLM multi-parameter probe (YSI Inc., Yellow Springs, OH, USA) including temperature (°C), turbidity (NTUs) and pH. Water clarity was determined as Secchi disk depth (SDD). Surface water grab samples were collected at each location at approximately 0.5 m below the water surface. Simultaneously, *in situ* spectral data were collected using ASD or Ocean Optics USB4000 spectrometers.

Spectral reflectance for the water bodies in Northeast China and East China were measured with an ASD spectrometer in accordance with the procedure proposed by Mobley (1999). Radiance was measured for both the water surface (L_{sw}) at approximately 1 m and a standard gray Spectralon (Labsphere, Inc., North Sutton, NH) reference panel (L_p) about 0.25 m above the panel. In order to effectively avoid the interference of boat wakes and the influence from direct solar radiance, the spectrometer was positioned at an azimuth angle of 135° and a zenith angle of 40°, which yields the optimal compromise among conflicting requirements (Mobley, 1999). The spectrometer was then rotated upwards by 90 ~ 120° to collect skylight radiance (L_{sky}). The viewing zenith angle was the same as that when measuring water radiance. The remote sensing reflectance (R_{rs}) could be calculated as:

$$R_{rs}(0^+, \lambda) = \frac{(L_{sw} - rL_{sky})\rho_p}{\pi L_p} \quad (1)$$

where r is the reflectivity of skylight at the air-water interface ($r = 0.028$ is acceptable for wind speed less than 5 ms⁻¹), and ρ_p represents reflectance of the gray Spectralon standard (30%).

The spectral reflectance for the water bodies in South Australia were collected using two inter-calibrated Ocean Optics USB4000 radiometers with CDAP/CALMIT programs developed by the University of Nebraska at Lincoln (Gitelson et al., 2008). The inter-calibration of the instruments was accomplished by measuring the upwelling radiance $L_{cal}(\lambda)$ from a 25% gray Spectralon reflectance standard and the corresponding incident irradiance $E_{cal}(\lambda)$ simultaneously. The above-water surface R_{rs} at nadir was computed as (Gitelson et al., 2008):

$$R_{rs}(0^+, \lambda) = \frac{tF(\lambda)L_{up}E_{cal}(\lambda)}{n^2\pi E_{inc}(\lambda)L_{cal}(\lambda)} R_{cal}(\lambda) \quad (2)$$

where t is the water-to-air transmittance and equals to 0.98, F is the spectral immersion factor computed following Ohde and Siegel (2003), n is the refractive index of water relative to air taken as 1.33, π is used to transform the irradiance reflectance R into a remote sensing reflectance, and $R_{cal}(\lambda)$ is the reflectance of the Spectralon panel linearly interpolated to match the band centers of each radiometer.

In situ spectra for the water bodies in Central Indiana, US for 2005 and 2006 were collected using an ASD spectrometer. Total upwelling radiance (L_{up}) was recorded with a fiber optic pointed in a nadir and was set at approximately 1.2 m above the water surface. Downwelling irradiance (E_d) measurements were collected at each sample site using a white Spectralon (99%). Remote sensing reflectance (R_{rs} ; sr⁻¹) was obtained using the ratio of upwelling radiance (L_{up} ; W.m⁻².sr⁻¹) at a nadir to the downwelling irradiance (E_d ; W.m⁻²):

$$R_{rs}(0^+, \lambda) = \frac{L_{up}(0^+, \lambda)}{E_d(0^+, \lambda)} \quad (3)$$

In this spectral measurement method, the impact of water-air interface and path radiance was not considered, however this might not have a significant effect on algorithms based on band ratios (Han and Rundquist, 1997; Doxaran et al., 2002).

2.3. Laboratory Analysis

Approximately 200 ~ 400 mL water samples were filtered onto pre-ashed and pre-weighed filters (47 mm, 0.7 µm pore size GF/F glass fiber filters) using a filtration manifold. TSM (mg/L) was calculated by subtracting the original weight of the clean filter from the post-filtered weight dried in 100 °C oven for 1 h. The filters used to measure TSM were weighed and then ashed for 75 min at 550 °C in a porcelain mu0 ffile furnace. Inorganic suspended matter (ISM, mg/L) was ca-

culated by subtracting the original weight of the filter from the post-ashed weight. Chl-a concentration was extracted in 90% buffer acetone and then determined spectrometrically following the EPA method (APHA, 1998), with details found in Song et al. (2012).

The TSM absorption coefficient was measured using a quantitative filter technique. First, each water sample was filtered using Whatman GF/FTM filters with a nominal pore size of 0.7 μm to measure the absorption spectrum of TSM (a_p). Second, organic pigments on the filters in the first step were removed using the methanol extraction method to measure the absorption spectrum of the depigmented samples (a_d). Subsequently, the spectral absorption coefficient for phytoplankton pigments a_{ph} was derived as the difference between a_p and a_d . A detailed description on how to determine the absorption of the various constituents can be found in the study by Cleveland and Weidemann (1993) and Xu et al. (2009).

2.4. Theory and TSM Modeling Methods

The bio-optical model based on Gordon et al. (1975) indicates that irradiance reflectance just beneath water surface $R(0)$ is closely related to the concentrations of water constituents, in which $R(0)$ is expressed as the ratio of the IOPs, i.e., total absorption (a) and backscattering (b_b) of OACs, and can be expressed as:

$$R(0^-, \lambda) = f \frac{b_b(\lambda)}{a(\lambda) + b_b(\lambda)} \quad (4)$$

where f denotes the experimental factor dependent on the light field (sun angle) and volume scattering function; and $a(\lambda)$ and $b_b(\lambda)$ are the total absorption and backscattering coefficients (m^{-1}) for a given wavelength, which are given by:

$$a(\lambda) = a_w(\lambda) + a_{ph}(\lambda) + a_{TR} + a_{CDOM}(\lambda) \quad (5)$$

$$b_b(\lambda) = b_{b,w}(\lambda) + b_{b,ph}(\lambda) + b_{b,TR}(\lambda) \quad (6)$$

where $a_w(\lambda)$, $a_{ph}(\lambda)$, $a_{TR}(\lambda)$, and $a_{CDOM}(\lambda)$ are the absorption coefficients for pure water, phytoplankton, TR denotes tripton, and CDOM at wavelength (λ), respectively, whereas $b_{b,w}(\lambda)$, $b_{b,ph}(\lambda)$, and $b_{b,TR}(\lambda)$ are the backscattering coefficients for corresponding components in a water column.

The primary objective of this study is to compare various empirical models for TSM estimation with data sets collected at various times and locations with a large concentration gradient. However, the relationships between water constituent IOPs and below-water reflectance, $R_{rs}(0^-, \lambda)$ and above water remote sensing reflectance $R_{rs}(0^+, \lambda)$, will help to explain these empirical models. Several studies have demonstrated that derivative analysis is an effective approach for TSM estimation using hyperspectral data (Chen et al., 1992; Han and Randquist, 1997), which can be derived from:

$$D_{\lambda(i)} = (R_{\lambda(j+1)} - R_{\lambda(j-1)}) / 2\Delta\lambda \quad (7)$$

where $D_{\lambda(i)}$ is the first derivative at a wavelength i midpoint between wavebands $j-1$ and $j+1$. $R_{\lambda(j-1)}$ and $R_{\lambda(j+1)}$ are reflectance at the $j-1$ and $j+1$ waveband and $\Delta\lambda$ is the difference in wavelengths (Pu and Gong, 2000). A 5-point triangular smooth algorithm was applied to the original spectral reflectance to reduce the noise before calculating the derivative of R_{rs} , which was implemented in Matlab 2009b software.

2.5. Model Accuracy Assessment

Different parameters between predicted value (y') and measured value (y) are calculated, including root mean square error (RMSE), relative RMSE (RMSE %), and mean absolute errors (MAE). The RMSE, MAE and relative error (RE), including its corresponding relative parameters are calculated by the following formula:

$$RMSE = \sqrt{\frac{\sum_{i=1}^N (y'_i - y_i)^2}{N}} \quad \text{and} \quad RMSE\% = 100 \times \frac{RMSE}{\bar{y}} \quad (8)$$

$$MAE = \frac{\sum_{i=1}^N |y'_i - y_i|}{N} \quad (9)$$

$$RE = 100 \times (y'_i - y_i) / y_i \quad (10)$$

where N is the number of samples in the dataset, and \bar{y} denotes the average measured value. Further, determination coefficient (R^2) and ratio of prediction to deviation (RPD) were applied in this study. As R^2 is a very common parameter its formula is omitted here, and RPD is calculated as (Miehle et al., 2006):

$$RPD = \frac{SDP}{\left(\sum (y' - y)^2 - \{[(y' - y)]^2 / N\} / (N - 1) \right)^{1/2}} \quad (11)$$

where SDP is determined by the follow equation:

$$SDP = \left\{ \sum y'^2 - [(y')^2 / N] / (N - 1) \right\}^{1/2} \quad (12)$$

According to Williams (2001), a model is accurate if R^2 and RPD values are above 0.91 and 2.5; a good prediction is achieved when R^2 ranges from 0.82 to 0.9 and RPD is higher than 2; whereas an approximate prediction is achieved when R^2 lies between 0.66 and 0.81 and RPD is higher than 1.5. Poor prediction is obtained when R^2 ranges from 0.5 to 0.65

Table 1. Descriptive Statistics of Water Quality Parameters

Parameter	Min	Max	Mean	SD	CV	N
(a) Field trips for Shitoukoumen Reservoir: Jun-28, Aug-17, Sep-12 and Oct-13 in 2006; May-21, Jun-22, Jul-19, Aug-28, Oct-12 in 2007; Jun-13, Sep-23 in 2008						
SDD (cm)	5	120	38	23.7	0.62	178
Turbidity (NTUs)	0.65	70.63	41.65	40.7	0.83	
TSM (mg/L)	3.67	225.2	58.78	54.78	0.84	
Chl-a ($\mu\text{g/L}$)	0.45	47.52	13.82	10.66	0.96	
Chl-a: TSM ($\mu\text{g/mg}$)	0.01	2.64	0.52	0.59	1.12	
(b) Field trips for Songhua Lake: May-11 in 2006, May-10, Jun-14, Sept-9, and Oct-13 in 2007; Jul-25 and Sept-24 in 2008						
SDD (cm)	86	755	252	108	0.43	156
Turbidity (NTUs)	0.03	15.22	2.09	2.12	1.04	
TSM (mg/L)	0.08	18.58	4.77	3.85	0.81	
Chl-a ($\mu\text{g/L}$)	0.45	37.52	8.82	7.66	0.87	
Chl-a: TSM ($\mu\text{g/mg}$)	0.43	21.81	2.91	3.59	1.23	
(c) Field trips for Chagan Lake: Jul-15, Aug-29 and Oct-12 in 2009; May-8 and Sept-13 in 2010						
SDD (cm)	11.5	50	32.1	10.72	0.34	99
Turbidity (NTUs)	30.52	95.55	67.21	52.03	0.77	
TSM (mg/L)	9.90	414.0	112.7	91.02	0.81	
ISM (mg/L)	5.3	378.6	79.37	76.33	0.96	
Chl-a ($\mu\text{g/L}$)	1.24	84.48	16.68	18.33	1.09	
Chl-a: TSM ($\mu\text{g/mg}$)	0.02	7.28	0.66	1.31	1.99	
(d) Field trips for Taihu Lake: October 2008 and May 2010						
SDD (cm)	12	180	52	32	0.61	94
TSM (mg/L)	1.57	68.1	28.4	23.7	0.83	
ISM (mg/L)	0.5	51.1	17.28	14.54	0.84	
Chl-a ($\mu\text{g/L}$)	0.46	183.2	28.82	27.92	0.96	
Chl-a: TSM ($\mu\text{g/mg}$)	0.23	12.34	1.56	2.41	1.54	
(e) Six field trips for three waters in South Australia during February 20 and March 4 in 2009						
SDD (cm)	20	275	96.2	79.6	0.83	60
Turbidity (NTUs)	0.80	41.50	13.07	11.16	0.85	
TSM (mg/L)	2.01	94.1	17.58	17.42	0.99	
Chl-a ($\mu\text{g/L}$)	6.27	75.3	19.09	13.46	0.70	
Chl-a: TSM ($\mu\text{g/mg}$)	0.62	5.51	1.84	1.28	0.69	
(f) Field trips for three reservoirs in Central Indiana, US: Sept-6-7 in 2005; Jun-15, Jun-29, Jul-6, Jul-19, Jul-25, Jul-31, Aug-1, Aug-16, Aug-22-24, Sept-7, Sept-19, Sept-25, Oct-6-7, Nov-2 in 2006						
SDD (cm)	24	150	62	32.4	0.52	276
Turbidity (NTUs)	2.3	42.0	9.3	4.2	0.45	
TSM (mg/L)	2.1	54.5	18.7	7.3	0.39	
ISM (mg/L)	0.8	33.1	8.7	4.6	0.52	
Chl-a ($\mu\text{g/L}$)	2.8	182.5	62.8	24.66	0.39	
Chl-a: TSM ($\mu\text{g/mg}$)	1.10	9.37	3.72	1.38	0.39	

* SDD, Secchi disk depth; TSM, total suspended matter; ISM, inorganic suspended matter; Chl-a, chlorophyll-a; SD, standard deviation and CV = (SD/average of parameters), coefficient of variation.

and RPD is below 1.5. In this study, all samples were organized in sequence according to their measured dates, and the first two were selected for calibration (2/3 of the samples), the third was chosen as validation (1/3 of the samples) for each dataset with the different modeling approaches.

3. Results

3.1. Constituent Characteristics

For all the field surveys conducted over 10 water bodies in the three countries, a large diversity of inland waters with varying OACs was encountered. The statistical values of the major water quality parameters, e.g., SDD, turbidity, TSM, and Chl-a for the various datasets are summarized in Table 1. TSM shows a wide range for the Shitoukoumen Reservoir (3.7 ~ 225.2 mg/L), resulting in lower water clarity and larger variation of turbidity. A similar trend is observed for Chagan Lake (TSM: 9.9 ~ 413.9 mg/L) with even lower water clarity and higher variation in turbidity. Medium concentration of TSM were observed in Taihu Lake and CIN waters from USA, but high Chl-a concentration with large variation occurred (Table 1). With concentration ranging from 0.08 to 18.58 mg/L, the TSM in Songhua Lake is low compared with those in the other waters being investigated.

As shown in Table 1, a large variability for the Chl-a: TSM ratio is observed within each water body. The lower Chl-a: TSM ratio for Shitoukoumen Reservoir and Chagan Lake suggest that these two are the most suspended-mineral-dominated waters. Lowest mean Chl-a: TSM ratio was observed for the Central Indiana samples because of the high Chl-a concentrations. The samples from both Taihu Lake and waters from South Australia are characterized by medium Chl-a: TSM ratios. As shown in Table 2, the correlation between TSM and Chl-a in the subsequent data sets varies significantly and the correlation coefficients (R) range from -0.26 to 0.93. For high TSM concentration water bodies, such as at the Shitoukou Reservoir and Chagan Lake, a low correlation is observed (Figure 1, Table 2), indicating Chl-a and TSM do not co-vary. In contrast, for the highly turbid productive waters, e.g., Taihu Lake, and waters from Central Indiana and South Australia, the TSM and Chl-a concentrations are closely associated (Table 2, Figure 1). For the aggregated dataset, a low correlation coefficient is observed (Table 2, Figure 1). The lack of a significant relationship between Chl-a and TSM for the aggregated data set indicates that each parameter plays different roles in affecting the optical properties of various water bodies (Gitelson et al., 2008), and TSM including phytoplankton is not fully co-varying with Chl-a concentration (Figure 1, Table 2).

3.2. Spectral Characteristics

In situ spectral measurements provide optical signatures over various waters bearing different TSM concentrations (Figures 2a-f). R_{rs} spectra, except from the Shitoukoumen Reservoir (Figure 2a) and Chagan Lake (Figure 2c), exhibit a shape quite similar to that collected in turbid productive waters

Table 2. Relationship of TSM and Chl-a concentration for various waters

Datasets	<i>N</i>	<i>R</i>	<i>P</i>	Regression	<i>R</i> ²
STKR	178	-0.26	>0.1	$Y = -0.329x + 1.517$	0.082
SHL	156	0.53	>0.05	$Y = 0.923x + 0.585$	0.220
CGL	99	-0.32	>0.05	$Y = -0.256x + 1.514$	0.087
THL	94	0.79	>0.001	$Y = 1.014x - 0.138$	0.696
SA	60	0.93	>0.001	$Y = 0.617x + 0.677$	0.808
CIN	276	0.70	>0.005	$Y = 1.090x + 0.405$	0.632
Aggregated	863	0.126	>0.5	$Y = 0.122x + 1.112$	0.016

* *N*, sample number; *R*, correlation coefficient between TSM and Chl-a; *P*, significant level; Regression, the dependent *Y* represents log (TSM) and independent *x* represents log (Chl-a) concentration; *R*², determination coefficient.

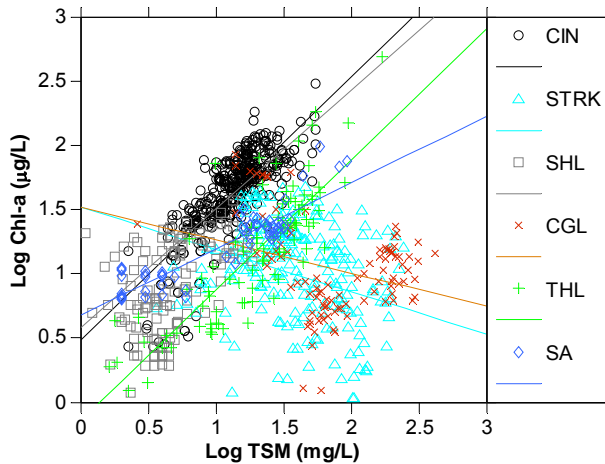


Figure 1. Scatter plot of logarithmic transformed total suspended matter (TSM) versus chlorophyll-a (Chl-a) concentrations for various datasets. CIN, three reservoirs in the Central Indiana, US; STKR, the Shitoukoumen Reservoir dataset; SHL, the Songhua Lake dataset; CGL, the Chagan Lake dataset; THL, the Taihu Lake dataset; SA, the South Australia datasets.

(Doxaran et al., 2002; Dall’Olmo and Gitelson, 2005). These water bodies, including the Taihu Lake (Figure 2d) and three reservoirs in Central Indiana (Figure 2f), are dominated by phytoplankton, exhibiting a deep absorption trough at approximately 680 nm. For the spectra collected over Songhua Lake (Figure 2b), most show low Chl-a and TSM concentration features, whereas the spectra from the Murray Rivers sections from South Australia (Figure 2e) show high TSM and Chl-a concentrations. The spectra from Myponga Reservoir (Figure 2e, low group) show low reflectance magnitude due to low TSM and Chl-a concentrations. The magnitude for the Shitoukoumen Reservoir and Chagan Lake exhibits high value at NIR region, which are consistent with spectra from highly turbid estuaries (Doxaran et al., 2002; Doron et al., 2011). A more remarkable variation in the spectral range of 750 ~ 900 nm suggests significant variability in TSM in the examined waters (Doxaran et al., 2002; Ruddick et al., 2006; Doron et al., 2011), as confirmed by the data presented in Table 2.

3.3. Correlation Analysis

Correlograms were constructed by sequential correlation analysis of reflectance, its derivative at each of 500 individual narrow bands against TSM concentration at a time, and subsequent plotting of the correlation coefficient (*R*) against wavelength for each dataset (Figure 3). The correlograms for TSM show broad regions of relatively high *R* value in both the visible and NIR spectral regions. Generally, the *R* value trends can be divided into three groups. The first group represents high TSM concentration, which shows high *R* values between 690 ~ 850 nm spectral region and non-algal particles dominating water upwelling radiance (Figure 3a and Figure 3c). The second group represents high algal and non-algal particle turbid waters (i.e. Figure 3d, 3e and 3f) with high *R* values at approximately 700 nm. The *R* value is generally relatively low in the blue, green, and NIR regions beyond 850 nm (Stumpf and Pennock 1989; Myint and Walker 2002). The third group represents low TSM concentration (i.e., Figure 2b), which exhibits high *R* values in the visible spectral region and relatively low *R* values between 650 ~ 850 nm (Binding et al., 2005).

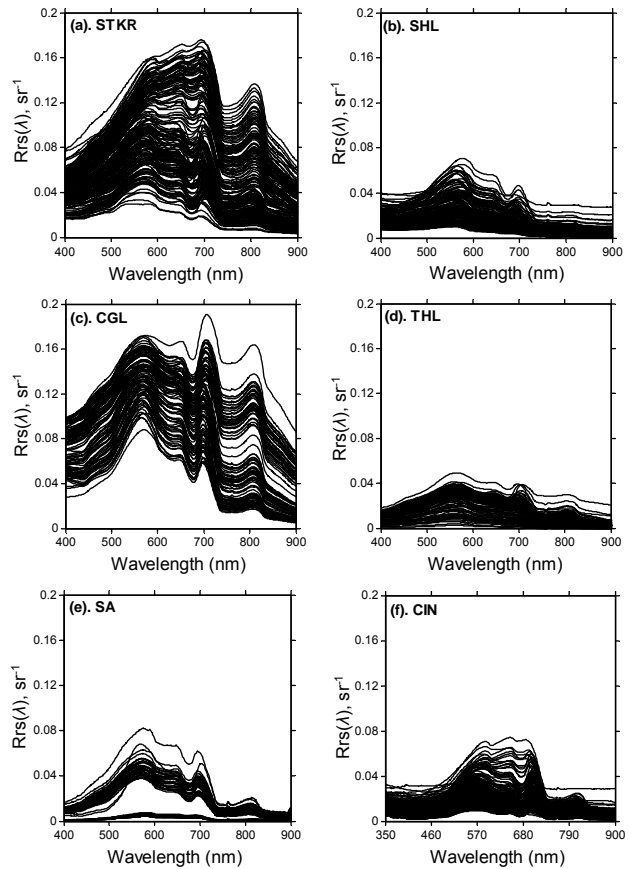


Figure 2. Remote sensing (*Rrs*) spectra for: (a) Shitoukoumen Reservoir; (b) Songhua Lake; (c) Chagan Lake; (d) Taihu Lake; (e) three drinking waters in South Australia with lower spectra collected from Myponga Reservoir (indicated by arrow), and (f) three reservoirs in Central Indiana, US.

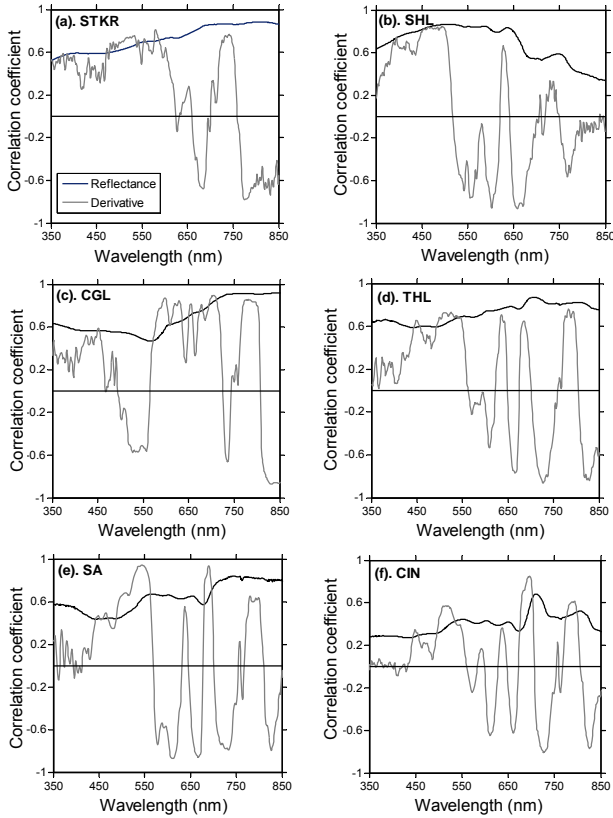


Figure 3. Total suspended matter (TSM) correlations with reflectance and derivative for each band with various datasets: (a) the Shitoukoumen Reservoir dataset; (b) the Songhua Lake dataset; (c) the Chagan Lake dataset; (d) the Taihu Lake dataset; (e) the South Australia dataset, and (f) dataset for three reservoirs in the Central Indiana, US.

The derivative reflectance obtains relatively high R values in the blue, green, and red regions, whereas relatively low values are observed in the NIR regions. The correlation coefficient fluctuated in both the visible and NIR regions, particularly in the blue and wavelength beyond 800 nm region. A significant variation for the R value of the collected datasets is illustrated in Figure 3. For waters from South Australia (Figure 3e) and Central Indiana (Figure 3f), derivative analysis proved to be an effective approach for improving TSM and spectral variable association. Hence, the highest R values are generally produced in the red spectral region (Chl-a fluorescence peak) for highly productive waters (i.e. Figure 3e-3f).

3.4. Band Ratio Analysis

For a preliminary analysis, 2-D coefficient correlograms were obtained by sequential regression of band ratio pairs ranging from 400 to 900 nm (250,000 combinations) against TSM concentrations (Figure 4). Several “hot spots” in the diagram indicate relatively broad regions of highly correlated band ratio with TSM concentrations. Apparently, large variations in the R values can be observed from various datasets, and the maximum values range from 0.81 (Figure 4b) to

0.97 (Figure 4e). The best performing band combination locations are not consistent for data sets collected from various waters. The overall pattern for the Shitoukoumen Reservoir (Figure 4a) is similar to that for the Chagan Lake (Figure 4c). This result is featured by the high R values in the spectral region beyond 700 nm and blue or green band ratio pairs. In terms of the data from the Songhua Lake, further investigation is necessary to elucidate the higher correlated band ratio pairs located in the red (around 690 nm) and blue spectral regions for TSM (around 400 nm). The highest correlation band ratio pairs for turbid productive waters usually occur at or around the chlorophyll absorption bands (Figures 4d-f). It can be noticed that both the Songhua and Taihu Lakes showed narrow band ratio windows with high R values, indicating limited band ratios can be applied for TSM estimation with remotely sensed data.

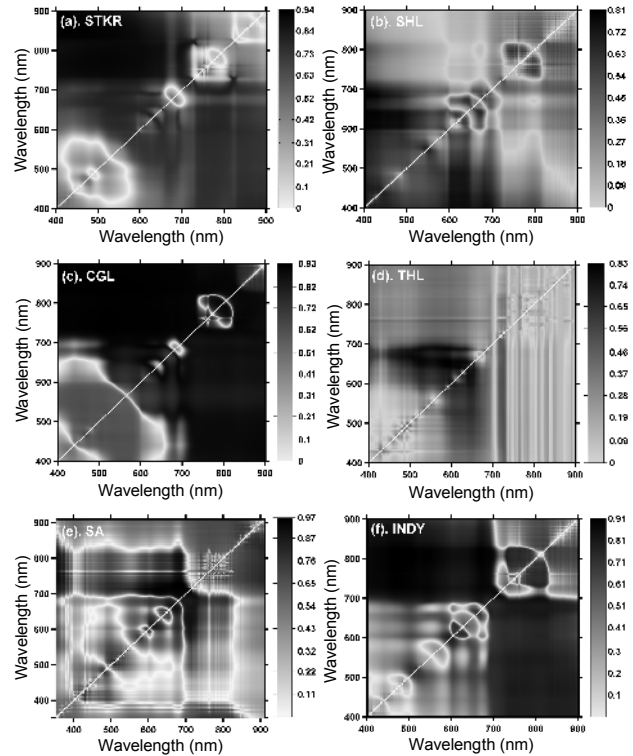


Figure 4. 2-D diagrams for total suspended matter (TSM) correlated with each band ratio pairs for various datasets: (a) the Shitoukoumen Reservoir dataset; (b) the Songhua Lake dataset; (c) the Chagan Lake dataset; (d) the Taihu Lake dataset; (e) the South Australia datasets, and (f) dataset for three reservoirs in the Central Indiana, US.

3.5. Model Performances

3.5.1. Various Data Sets

The empirical models based on the optimal band ratios (OBR) for TSM with various datasets are presented in Figures 5a-f, whereas the model accuracy parameters are summarized in Table 3. The models based on the OBR perform well with both calibration and validation samples evenly dis-

tributed along the 1:1 line for the Shitoukoumen Reservoir and South Australia data sets. The model predictions are accurate according to the criteria proposed by Williams (2001) as shown by the R^2 and RPD values (Table 3). The OBR model for SA dataset performs best among all datasets, and it also performs well with the Chagan Lake data set, except for three outliers. A good model prediction is obtained with respect to R^2 and RPD (Table 3). The OBR model performs poorly according to the given criteria for the Songhua Lake data set with low R^2 and a slope far from unity (0.64). The OBR models for Taihu Lake and Central Indiana data sets achieve approximate prediction according to the R^2 and RPD values in Table 3. Both models showed a non-linear relationship between measured and predicted TSM, especially when TSM concentration was more than 30 mg/L (Figures 5d and f).

Modeling results based on the sensitive band reflectance (SB), derivative (SD), and DM are summarized in Table 3. The models based on different spectral variables perform well for the highly turbid Shitoukoumen Reservoir and Chagan Lake. The DM shows similar prediction performance to OBR, and both outperformed the SB and SD models (Table 3). Nevertheless, the DM models for the other waters, i.e. Songhua Lake, Taihu Lake, and waters from South Australia and Central Indiana, with lower TSM and high algal particles perform poorly (Table 3). The SB (the spectral bands are STKR: 853 nm; SHL: 557 nm; CGL: 776 nm; THL: 713 nm; SA: 743 nm and CIN: 711 nm, respectively) and SD (the corresponding bands are STKR: 630 nm; SHL: 652 nm; CGL: 880 nm; THL: 727 nm; SA: 690 nm and CIN: 698 nm, respectively) models achieve stable performances, whereas some models (THL and CIN datasets) achieve accuracy close to that of the OBR model, and are even better for the SHL dataset.

3.5.2. Aggregated Dataset

The performances of the four modeling approaches are compared with the aggregated data set ($n = 863$), and the results are illustrated in Figure 6. The four models exhibit relatively similar performances with the aggregated data set. The correlation between the measured and the model-predicted results fitted well along the 1:1 line except for the three samples from Chagan Lake (Figure 6a). The slope close to unity and small intercept values (2.037 mg/L) further confirm that the OBR model achieved good performance. The RMSE of TSM prediction is 14.6 mg/L for the OBR model, with a systematic overestimation or underestimation when TSM concentrations are less than 20 mg/L (Figure 6b). Generally, the relative error (RE) is reduced when TSM concentration increases (Table 4). The DM model performs well for some waters, the model-predicted and measured TSM concentrations correlate well with the aggregated dataset (Figure 6c). However, the model achieves smaller slope (0.89) and slightly larger intercept values, showing lower determination coefficient ($R^2 = 0.87$) and higher RMSE value (17.25 mg/L). Similar to the OBR model, a systematic RE is observed when TSM concentration is less than 20 mg/L (Figure 6d). The SB and SD models show performances similar to that of

the DM model considering their respective RMSEs (20.17 and 18.30 mg/L), determination coefficients (0.87 and 0.88), and intercepts (4.02 and 4.42), but with varied respective slope values (0.98 and 0.88) (Figures 6e and 6g). The RE values for the SB and SD models are also comparable, as shown in Figures 6f and 6h for the aggregated dataset.

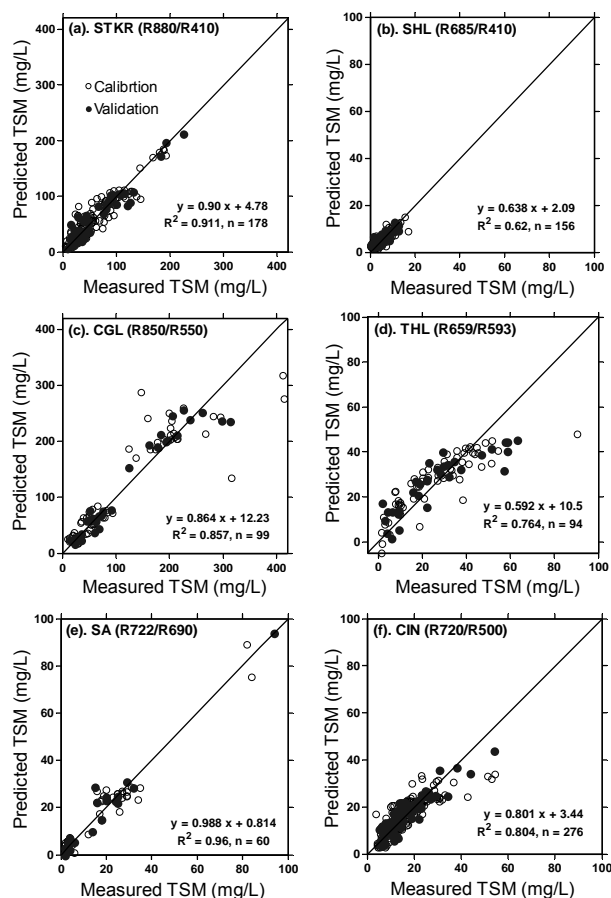


Figure 5. Correlation between measured and predicted TSM for various datasets with specific band ratios: (a) the Shitoukoumen Reservoir dataset; (b) the Songhua Lake dataset; (c) the Chagan Lake dataset; (d) the Taihu Lake dataset; (e) the South Australia dataset, and (f) the dataset from three reservoirs in Central Indiana, US.

As shown in Table 4, variable performances were observed for different models with respect to different TSM ranges. Better performance was observed for SD in the TSM range of 0 ~ 10 mg/L ($N = 254$), while largest mean RE value was achieved with DM (Table 4). In the TSM range of 10 ~ 50 mg/L ($N = 458$) and 50 ~ 100 mg/L ($N = 87$), the lowest mean RE value was achieved through the OBR modeling approach. Nevertheless, similar mean RE values were derived from OBR, DM and SD modeling approaches when the TSM concentration was greater than 100 mg/L (Table 4). Thus, it can be seen that SD is effective for TSM estimation with lower concentrations in the water column, while OBR performs well for TSM with medium concentration ranges.

Table 3. Results of Calibration and Validation for Various Models Using Different Datasets

Models	Model calibration					Model validation				
	RMSE	RMSE%	MAE	RPD	R ²	RMSE	RMSE%	MAE	RPD	R ²
(a) Dataset for Shitoukoumen Reservoir Northeast China:										
OBR	15.9	28.2	11.9	4.5	0.89	14.1	24.5	10.7	5.3	0.92
DM	20.2	35.6	15.0	3.6	0.79	16.6	29.0	12.9	4.5	0.88
SB	20.7	35.9	14.7	3.5	0.78	20.5	35.7	14.6	3.5	0.78
SD	23.7	38.4	19.2	3.1	0.69	23.9	39.0	19.5	3.0	0.69
(b) Dataset for Songhua Lake in Northeast China:										
OBR	1.8	37.6	1.3	3.2	0.68	2.6	37.9	1.5	2.9	0.65
DM	2.7	55.5	1.9	2.2	0.31	16.6	54.2	1.9	2.0	0.25
SB	18.2	31.7	15.2	3.3	0.75	18.0	31.5	15.0	3.3	0.75
SD	18.6	32.8	15.7	3.2	0.73	18.2	32.1	15.2	3.4	0.74
(c) Dataset for Chagan Lake in Northeast China:										
OBR	41.2	36.0	23.4	3.7	0.83	23.6	20.8	15.2	6.2	0.93
DM	41.6	36.4	23.9	3.6	0.82	23.5	20.5	15.7	6.2	0.93
SB	42.1	36.6	23.7	3.5	0.82	42.8	36.4	23.8	3.4	0.81
SD	41.6	36.3	23.5	3.7	0.83	41.5	36.2	23.6	3.7	0.83
(d) Dataset for Taihu Lake in East China:										
OBR	10.0	39.1	7.0	3.1	0.67	9.8	37.5	7.9	3.3	0.76
DM	15.5	60.5	11.4	2.0	0.21	18.0	68.0	13.2	1.8	0.09
SB	10.1	37.9	8.1	3.2	0.75	9.4	37.2	7.7	3.4	0.77
SD	9.9	37.7	8.0	3.2	0.75	10.7	38.2	8.3	3.1	0.73
(e) Dataset for three drinking water sources in South Australia:										
OBR	4.6	24.9	3.5	5.7	0.94	4.2	22.6	2.9	6.5	0.96
DM	17.0	92.3	9.8	1.5	0.17	19.6	104.1	10.9	1.4	0.09
SB	7.2	32.5	5.9	3.7	0.70	6.9	31.1	5.4	3.9	0.73
SD	5.3	26.1	3.9	4.8	0.88	5.1	26.9	3.7	5.1	0.90
(f) Dataset for three drinking water source in central Indiana, US:										
OBR	4.9	30.2	3.4	3.6	0.66	3.7	22.8	2.9	4.9	0.80
DM	8.0	49.9	5.5	2.3	0.08	7.9	49.2	5.6	2.3	0.10
SB	4.3	27.4	3.1	4.1	0.74	4.5	28.2	3.2	3.9	0.72
SD	6.1	37.8	4.2	3.2	0.46	5.7	35.1	3.8	3.4	0.52

* OBR, model based on optimal band ratio through iteration; DM, model based on Doxaran et al. (2002) proposed bands (R850/R550); SB, model based on sensitive spectral band; SD, model based on sensitive derivative.

4. Discussion

4.1. Performance Comparison

It can be observed from Table 3 that four modeling approaches perform well for highly turbid waters with abundant TSM in the water column. Compared to the STKR, more inorganic matter exists in the CGL water (Table 1). Therefore four modeling approaches perform well due to stronger water-leaving radiance. For highly productive waters, e.g., the three reservoirs from Central Indiana, Taihu Lake, and waters from South Australia, the OBR model significantly outperforms the DM model (Table 3), and marginally outperforms SB and SD models. For the SHL, a more clear water (average SDD: 2.09 m) with low TSM (Table 1), SB and SD models achieve relative better performance than OBR and DM; the DM model yields a low R² of 0.25.

As shown in Figure 6, four of the models all yield good results with the aggregated dataset, in which the OBR marginally outperforms the other three models (Table 4). As noted, this is likely because the large TSM concentration gradient

from the Chagan Lake and Shitoukoumen Reservoir covering the TSM range from other waters; thereby DM also shows good predicted result for the aggregated dataset. It is evident from Figure 6b, 6d, 6f and 6h that the OBR modeling approach yields lower relative error (35.8%), DM yields higher RE (65.7%), while medium REs are observed for SB (41.2%) and SD (39.0%) modeling, suggesting that OBR is the best among these four modeling approaches. Different TSM ranges also confirm this conclusion (Table 4).

Variability in TSM composition results in differences in the dominant OACs and the relationship between TSM and spectral variables (i.e., spectral reflectance, derivative, and band ratio) varies significantly. Aside from the variations in sediment types (grain size and mineral refractive index) and illumination conditions, all parameters can affect the water-leaving signal of inland waters and the accuracy of remotely sensed TSM concentrations (Chen et al., 1992; Doxaran et al., 2003; Sváb et al., 2005). Although the derivative analysis and band ratios of NIR and visible regions can partly reduce or

eliminate the aforementioned effects, they cannot fully cover these diverse compositional variations in OACs (Doxaran et al., 2002, 2003, 2005; Binding et al., 2005; Nechad et al., 2010). The DM model works well for waters with high TSM concentration dominated by non-algal particles (Figures 5a and c).

Table 4. Statistics for Relative Errors with Respect to Different TSM Concentration Ranges for Optimal Band Ratio (OBR), Doxaran Model (DM, Doxaran et al., 2002), Sensitive Spectral Band (SB) and Sensitive Derivative Reflectance (SD) Models for Aggregated Dataset

TSM (mg/L)	Samples (N)	Statistics	OBR	DM	SB	SD
0-10	254	Min	-405.07	-60.31	-142.38	-562.30
		Max	955.97	1105.65	1188.49	1046.42
		Mean	69.16	147.32	65.27	63.92
		SD	141.08	327.94	143.29	150.90
10-50	458	Min	-63.62	-73.03	-57.71	-187.20
		Max	225.34	296.55	290.08	379.91
		Mean	25.20	31.91	31.39	30.65
		SD	35.50	42.72	47.34	45.87
50-100	87	Min	-47.12	-81.75	-65.27	-152.17
		Max	62.10	86.68	155.42	118.28
		Mean	18.11	27.55	38.70	29.40
		SD	22.38	34.68	46.21	39.38
>100	68	Min	-54.62	-57.64	-61.03	-66.84
		Max	96.20	94.32	88.72	75.64
		Mean	14.04	16.07	20.90	16.47
		SD	22.10	21.87	26.05	21.49

* Min, denotes minimum value; Max, denotes maximum value, and SD represents standard deviation. # indicates that the mean value and is calculated through the absolute relative errors (RE) to avoid the cancelation of positive and negative values.

4.2. Chl-a vs. Relative Error

Investigations have proven that non-phytoplankton absorption, such as detritus and CDOM, may cause a tendency of Chl-a overestimates (Gons, 1999; Gitelson et al., 2008; Yang et al., 2011). The same is true for TSM estimation because phytoplankton tends to reduce spectral reflectance in the visible spectral region (400 ~ 690 nm) as illustrated by Sváb et al. (2005, Figure 6). An example of this condition is presented in Figure 7a, where three spectra had practically similar TSM concentrations (35.7, 34.8, and 34.25 mg/L) but with distinct Chl-a concentrations (24.93, 36.23, and 53.55 µg/L). Higher phytoplankton abundance increases the absorption, which in turn causes Rrs reduction in the spectral range of 400 ~ 700 nm with significantly larger magnitudes than that in the spectral range of 700 ~ 900 nm. Consequently, an overestimation of TSM is observed for samples with higher Chl-a concentrations (TSM_{predicted} = 36.15, 37.23, and 40.24 mg/L) derived from the DM model. Similar trends are found with OBR and SB modeling.

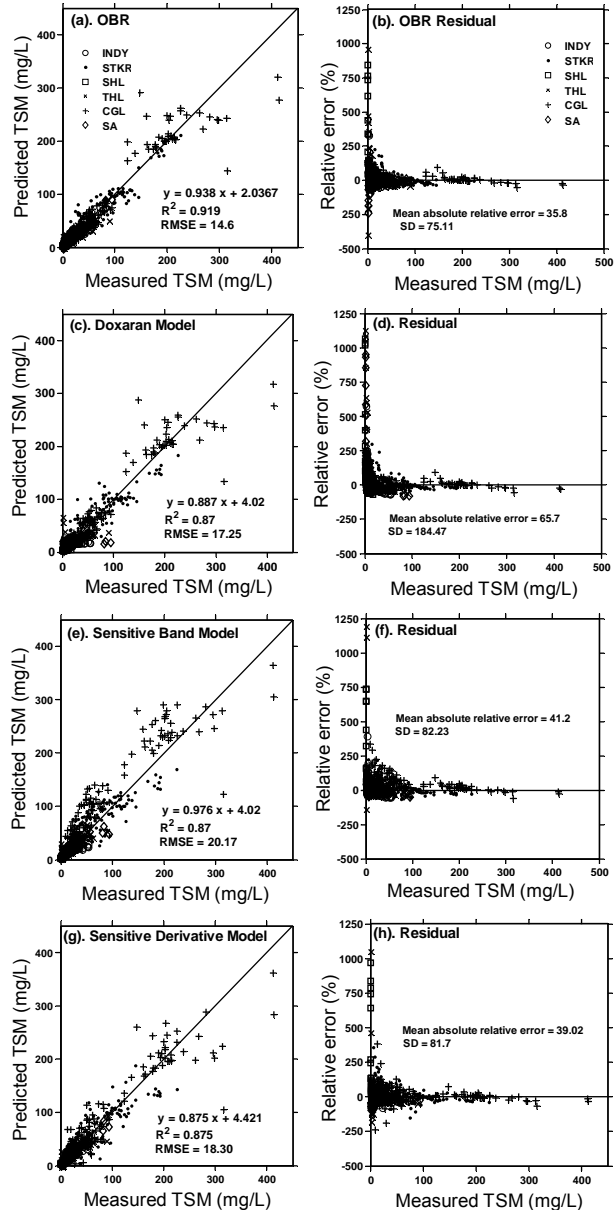


Figure 6. Comparison of various modeling approaches for aggregated datasets: (a) optimal band ratio model and (b) relative error (RE) vs TSM in the first row; (c) Doxaran Model result and (d) RE vs TSM in the second row; (e) sensitive spectral band model and (f) RE vs TSM in the third row; (g) sensitive derivative model, and (h) RE vs TSM in the fourth row. SD: standard deviation.

To analyze the influence of Chl-a concentration on TSM estimation based on band ratio algorithms, the HydroLight software (Sequoia Scientific, Inc., Bellevue, WA) was used to simulate Rrs with various Chl-a and ISM combinations (Gitelson et al., 2007; Yang et al., 2011). Laboratory-measured IOPs, such as a_{ph} , a_{TR} , and a_{CDOM} from Equations (5) and (6), are provided as inputs for the HydroLight simulation, whereas the default case-II water scenarios are considered for the simulation of b_b . ISM concentration changes from 1 to 500

mg/L with 10 mg/L increment intervals, and Chl-a concentration changes from 1 to 500 µg/L with 10 µg/L increment intervals. A ratio between algal dry biomass and Chl-a of 100 is adopted in this study (Aponasenko et al., 2007) to convert Chl-a concentration into dry weight of total phytoplankton. The influence of Chl-a concentration variation on TSM estimation using the OBR modeling approach is illustrated in Figure 7b. Phytoplankton abundance causes remarkable variation for the band ratio at the same TSM concentration level through simulated Rrs. A power regression fitted the TSM well with the simulated dataset, which is in good agreement with the results from Doxaran et al. (2002, 2005).

Figure 7c indicates that the Chl-a concentration exerts a varied influence on various ISM concentrations. The lower the Chl-a concentration, the stronger the influence Chl-a exerts on OBR for TSM estimation. 51 groups of Chl-a are regressed (with both linear and non-linear regressions) against OBR to analyze the influence of phytoplankton abundance on TSM estimation. It can be observed from Figure 7d that the modeling R-square values are less influenced with lower Chl-a concentration, while the slightly stronger influences are observed when the Chl-a concentrations increase, particularly when the concentration reaches 200 µg/L. A more systematic dataset is still needed to further confirm this assumption in future work, particularly with *in situ* collected datasets. The effects of phytoplankton composition and package (Bricaud et al., 1995; Babin et al., 2003) are other issues that also should be considered for TSM estimation for inland turbid productive waters, in addition to CDOM with the visible band (Bricaud et al., 1995; Babin et al. 2003; Yang et al., 2011). Similar patterns are also observed for DM and SB, but SD is more effective to reduce the Chl-a effect on TSM estimation.

Figure 8a shows the relationship between absolute values for relative error (RE) and Chl-a concentration. No obvious correlation ($R = 0.17$) can be observed for the *in situ* dataset. Analysis reveals that the correlation between absolute values of RE and Chl-a concentration varies for different datasets, and the R values are 0.054 (STKR), 0.251 (SHL), 0.362 (CGL), 0.338 (THL), 0.469 (SA), 0.026 (CIN), respectively. It has been proven that pigment absorption efficiency is a function of season, environment conditions, nutrient and light availability, and species composition (Metsamaa et al., 2006; Randolph et al., 2008; Paerl and Paul, 2012). Similarly, the absorption of non-algal particle also varies due to the composition, particles size and concentration (Babin et al., 2003; Binding et al., 2005). Figure 8b shows the correlation between absolute values of RE and Chl-a: TSM ratio, an obvious trend ($R = 0.53$) can be observed that samples with high Chl-a: TSM ratios usually account for high RE values. Similarly, the correlation between RE and Chl-a: TSM ratio varies for different datasets, and the correlation coefficients are 0.394 (STKR), 0.723 (SHL), 0.706 (CGL), 0.308 (THL), 0.685 (SA), 0.331 (CIN). The variations are most probably due to the association among various OACs in the different waters. It is worth noting that the relative concentration of Chl-a to TSM ratio exerts impact on the TSM modeling accuracy.

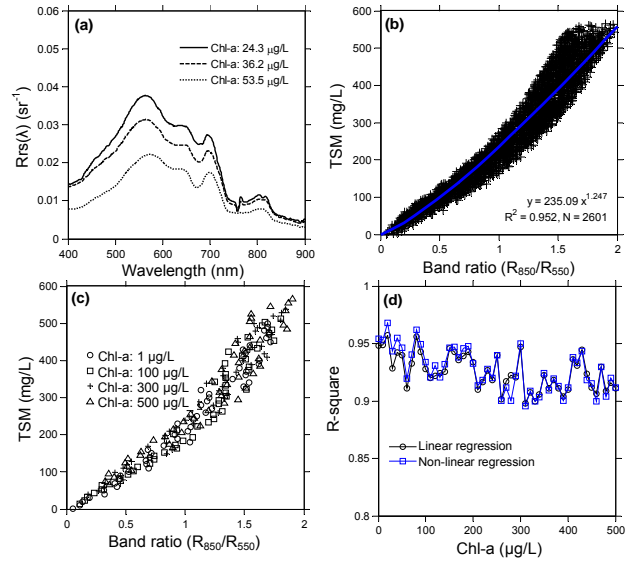


Figure 7. Influence of Chl-a concentration on TSM estimation based optimal band ratio (OBR) algorithm: (a) remote sensing reflectance spectra taken in Lake Taihu, TSM concentration is 35.7, 34.8 and 34.25 mg/L while Chl-a concentration is 24.93, 36.23 and 53.55 µg/L, respectively; (b) Chl-a concentration influence on TSM estimation through Hydro-light simulated remote sensing reflectance, ISM ranges [1, 500] with 10 mg/L increment interval and Chl-a ranges [1, 500] with 10 µg/L interval; (c) relationship between OBR band ratio and TSM under the influence of some specific Chl-a concentrations; (d) determination coefficient variation via OBR modeling approach against Chl-a concentration changing from 1 to 500 µg/L with 10 µg/L interval.

4.3. Performances vs. IOPs

As shown in Figures 3 to 5 and Table 3, different sensitive reflectance bands, derivatives, and band ratios are observed for various waters because of the variations in the composition of OACs (Doxaran et al., 2003; Binding et al., 2005; Doron et al., 2011). According to previous investigations (Gordon et al., 1975; Morel and Gentili, 1993), back-scattering coefficient (bb) determines the R_{rs} magnitude, thus higher R_{rs} spectra from Shitoukoumen Reservoir and Chagan Lake are mainly determined by high bb values. However, no bb values were measured in this study, which restrict us from in-depth discussion on this aspect. According to our results, four modeling approaches achieve stable performances for the Shitoukoumen Reservoir and Chagan Lake data sets. Non-algal substances in Chagan Lake contributed more than 80% of the absorption for all TSM absorption (Figure 9). Even for the Shitoukoumen Reservoir, the phytoplankton shows nearly equal absorption to non-algal absorption only in a very narrow spectral region around 620 nm (Figure 9). Further, it is also indicated from Figure 1 and Table 2 that TSM and Chl-a are less correlated, which are different from the other data sets (see regression lines in Figure 1 for CIN, THL, SA and SHL data sets). Analysis of the relative contributions of algal and non-algal particles to TSM absorption indicates that phytoplankton accounts for nearly half of the TSM absorption in

Songhua Lake (Figure 10 black line), implying that pigments contribute a large proportion to TSM absorption, especially in the spectral region of 600 ~ 700 nm (Lohrenz et al., 2003). In contrast, the relative contributions of algal and non-algal particles to absorption indicate that phytoplankton accounts for most of the TSM total absorption in the waters from Central Indiana, USA (Figure 10), implying phytoplankton dominate the total TSM absorption.

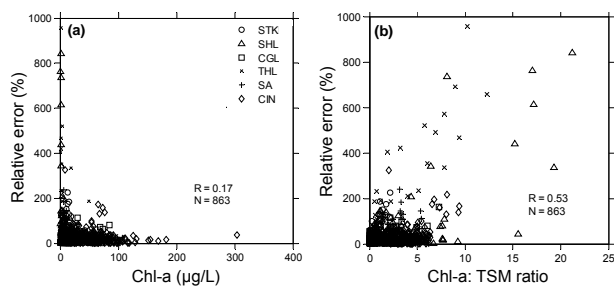


Figure 8. The relationship between (a) absolute RE and Chl-a concentration, (b) absolute RE values and the concentration ratio of Chl-a: TSM.

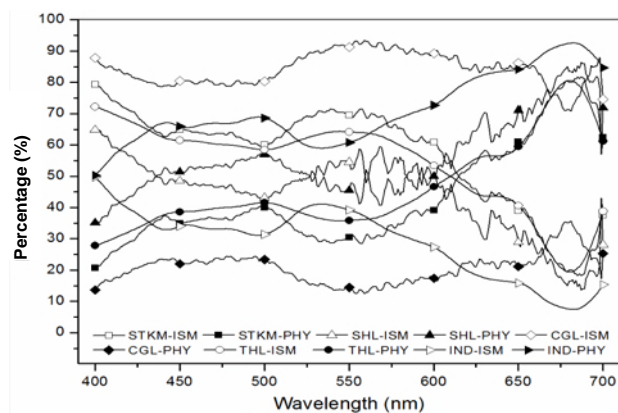


Figure 9. Relative contributions of inorganic suspended matter (ISM) and phytoplankton to the TSM absorption spectra in various water bodies.

5. Conclusions

Numerous *in situ* reflectance measurements covering a diverse range of TSM and phytoplankton abundance were collected for remotely estimating TSM using spectral data. The models perform better with four approaches when the waters are dominated by non-algal particulate matter with higher TSM concentrations (e.g., the STKR and CGL data sets). However, the DM model performs poorly when the waters are dominated by phytoplankton, as well as at low TSM concentration (e.g., the SHL data set) because the model is originally developed for highly turbid estuarine waters with relatively low Chl-a concentration. To summarize, the OBR model works well for waters with variable TSM concentration, SB and SD models also achieve reasonable accuracy for TSM estimates.

Our results indicate that the band ratio algorithm becomes nonlinear for highly productive waters (e.g., THL and CIN waters) when phytoplankton dominates the spectral absorption feature. Phytoplankton abundance in the water column can complicate water-leaving spectral signals, which may limit or reduce the accuracy of the algorithm for remote sensing of TSM concentration. Remote sensing models based on the classification of waters according to AOPs, such as Rrs or IOPs (a and b_b), should be considered in future research because grouping waters with similar AOPs or IOPs may facilitate TSM estimation through remote sensing technology for inland water (Lubac and Loisel, 2007). Thereby, various models oriented to variable water types can be established for accurately estimating TSM in the water column using remotely sensed data.

Acknowledgements. The authors would like to thank all the students and faculty from various organizations participating in the sampling excursions and the laboratory analyses. This research was supported by a NSFC fund granted to Dr. Kaishan Song (No.4117-1293) and a NASA fund granted to Dr. Lin Li (NNG06GA92G). Many thanks also go to two anonymous reviewers for their valuable comments.

References

- Acker, J., Ouillon, S., Gould, R., and Arnone, R. (2005). Measuring marine suspended sediment concentrations from space: history and potential. Paper presented at the 8th International Conference on Remote Sensing for Marine and Coastal Environments, Halifax, NS, Canada.
- APHA/AWWA/WEF. (1998). Standard methods for the examination of water and wastewater. Washington, D.C: American Public Health Association.
- Aponasenko, A.D., Shchur, L.A., and Lopatin, V.N. (2007). Relationship of the Chlorophyll Content with the Biomass and Disperse Structure of Phytoplankton. *Dokl. Biol. Sci.*, 412, 61-63. <http://dx.doi.org/10.1134/S0012496607010206>
- Babin, M., Stramski, D., Ferrari, G.M., Claustre, H., Bricaud, A., Obolensky, G., and Hoepffner, N. (2003). Variations in the light absorption coefficients of phytoplankton, nonalgal particles and dissolved organic matter in coastal waters around Europe. *J. Geophys. Res.*, 108(7), 3211. <http://dx.doi.org/10.1029/2001JC000882>
- Binding, C.E., Bowers, D.G., and Mitchelson, E.G. (2005). Estimating suspended sediment concentrations from ocean colour observations in moderately turbid waters: the impact of variable particle scattering properties. *Remote Sens. Environ.*, 94, 373-383. <http://dx.doi.org/10.1016/j.rse.2004.11.002>
- Brando, V.E., and Dekker, A.G. (2003). Satellite hyperspectral remote sensing for estimating estuarine and coastal water quality. *IEEE Trans. Geosci. Remote Sens.*, 41, 1378-1387. <http://dx.doi.org/10.1109/TGRS.2003.812907>
- Bricaud, A., Babin, M., Morel, A., and Claustre, H. (1995). Variability of chlorophyll specific absorption coefficient of natural phytoplankton analysis and parameterize. *J. Geophys. Res.*, 100(C7), 13321-13332. <http://dx.doi.org/10.1029/95JC00463>
- Chen, Z.M., Curran, P.J., and Hanson, J.D. (1992). Derivative reflectance spectroscopy to estimate suspended sediment concentration. *Remote Sens. Environ.*, 40, 67-77. [http://dx.doi.org/10.1016/0034-4257\(92\)90127-6](http://dx.doi.org/10.1016/0034-4257(92)90127-6)
- Cleveland, J.S., and Weidemann, A.D. (1993). Quantifying absorption by aquatic particles: a multiple scattering correction for glass-

- fiber filter. *Limnol. Oceanogr.*, 38, 1321-1327. <http://dx.doi.org/10.4319/lo.1993.38.6.1321>
- Dall'Olmo, G., and Gitelson, A.A. (2005). Effect of bio-optical parameter variability on the remote estimation of chlorophyll-a concentration in turbid productive waters: Experimental results. *Appl. Optics*, 44, 412-422. <http://dx.doi.org/10.1364/AO.44.000412>
- Dekker, A.G., Vos, R.J., and Peters, S.W.M. (2001). Comparison of remote sensing data, model results and in situ data for total suspended matter (TSM) in the southern Frisian lakes. *Sci. Total Environ.*, 268 (1-3), 197-214. [http://dx.doi.org/10.1016/S0048-9697\(00\)00679-3](http://dx.doi.org/10.1016/S0048-9697(00)00679-3)
- Dekker, A.G., Vos, R.J., and Peters, S.W.M. (2002). Analytical algorithms for lake water TSM estimation for retrospective analyses of TM and SPOT sensor data. *Int. J. Remote Sens.*, 23(1), 15-35. <http://dx.doi.org/10.1080/01431160010006917>
- Doron, M., Bélanger, S., Doxaran, D., and Babin M. (2011). Spectral variations in the near-infrared ocean reflectance. *Remote Sens. Environ.*, 115, 1617-1631. <http://dx.doi.org/10.1016/j.rse.2011.01.015>
- Doxaran, D., Froidefond, J.M., Lavender, S., and Castaing, P. (2002). Spectral signature of highly turbid waters Application with SPOT data to quantify suspended particulate matter concentrations. *Remote Sens. Environ.*, 81, 149-161. [http://dx.doi.org/10.1016/S0034-4257\(01\)00341-8](http://dx.doi.org/10.1016/S0034-4257(01)00341-8)
- Doxaran, D., Froidefond, J.M., and Castaing, P. (2003). Remote sensing reflectance of turbid sediment-dominated waters. Reduction of sediment type variations and changing illumination conditions effects using reflectance ratios. *Appl. Optics*, 42, 2623-2634. <http://dx.doi.org/10.1364/AO.42.002623>
- Doxaran, D., Cherukuru, R.C.N., and Lavender, S.J. (2005). Use of reflectance band ratios to estimate suspended and dissolved matter concentrations in estuarine waters. *Int. J. Remote Sens.*, 26(8), 1763-1769. <http://dx.doi.org/10.1080/01431160512331314092>
- Doxaran, D., Cherukuru, R.C.N., and Lavender, S.J. (2006). Inherent and apparent optical properties of turbid estuarine waters: measurements, modelling and application to remote sensing. *Appl. Optics*, 45, 2310-2324. <http://dx.doi.org/10.1364/AO.45.002310>
- Fettweis, M., Francken, F., Pison, V., and Eynde, V.D.D. (2006). Suspended particulate matter dynamics and aggregate sizes in a high turbidity area. *Mar. Geol.*, 235, 63-74. <http://dx.doi.org/10.1016/j.margeo.2006.10.005>
- Forget, P., Ouillon, S., Lahet, F., and Broche, P. (1999). Inversion of reflectance spectra of nonchlorophyllous turbid coastal waters. *Remote Sens. Environ.*, 68, 264-272. [http://dx.doi.org/10.1016/S0034-4257\(98\)00117-5](http://dx.doi.org/10.1016/S0034-4257(98)00117-5)
- Gilerson, A., Zhou, J., Hlaing, S., Ioannou, I., Schalles, J., Gross, B., Moshary, F., and Ahmed, S. (2007). Fluorescence component in the reflectance spectra from coastal waters dependence on water composition. *Optics Express*, 15(24), 15702-15721. <http://dx.doi.org/10.1364/OE.15.015702>
- Gitelson, A.A., Dall'Olmo, G., Moses, W., Rundquist, D.C., Barrow, T., Fisher, T. R., Gurlin, D., and Holz, J. (2008). A simple semi-analytical model for remote estimation of chlorophyll-a in turbid waters: Validation. *Remote Sens. Environ.*, 112, 3582-3593. <http://dx.doi.org/10.1016/j.rse.2008.04.015>
- Gordon, H.R., Brown, O.B., and Jacobs, M.M. (1975). Computed relationship between the inherent and apparent optical properties of a flat homogeneous ocean. *Appl. Optics*, 14, 417-427. <http://dx.doi.org/10.1364/AO.14.000417>
- Gons, H.J. (1999). Optical teledetection of chlorophyll a in turbid inland waters. *Environ. Sci. Technol.*, 33, 1127-1132. <http://dx.doi.org/10.1021/es9809657>
- Han, L.H., Rundquist, D.C., Liu, L.L., Fraser, R.N., and Schalles, J.F. (1994). The spectral responses of algal chlorophyll in water with varying levels of suspended sediment. *Int. J. Remote Sens.*, 15, 3707-3718. <http://dx.doi.org/10.1080/01431169408954353>
- Han, L.H., and Rundquist, D.C. (1997). Comparison of NIR/RED ratio and first derivative of reflectance in estimating algal-chlorophyll concentration: a case study in a turbid reservoir. *Remote Sens. Environ.*, 62, 253-261. [http://dx.doi.org/10.1016/S0034-4257\(97\)00106-5](http://dx.doi.org/10.1016/S0034-4257(97)00106-5)
- Hans, H., Haan, J., Jordans, R., Vos, R., Peters, S., and Rijkeboer, M. (2002) Towards airborne remote sensing of water quality in The Netherlands—validation and error analysis. *ISPRS J. Photogramm. Remote Sens.*, 57(3), 171-183. [http://dx.doi.org/10.1016/S0924-2716\(02\)00120-X](http://dx.doi.org/10.1016/S0924-2716(02)00120-X)
- Hu, C., Chen, Z., Clayton, T.D., Swarzenski, P., Brock, J.C., and Muller-Karger, F.E. (2004). Assessment of estuarine water-quality indicators using MODIS medium-resolution bands: Initial results from Tampa Bay, FL. *Remote Sens. Environ.*, 93, 423-441. <http://dx.doi.org/10.1016/j.rse.2004.08.007>
- Lohrenz, S.E., Weidemann, A.D., and Tuel, M. (2003). Phytoplankton spectral absorption as influenced by community size structure and pigment composition. *J. Plankton Res.*, 25(1), 35-61. <http://dx.doi.org/10.1093/plankt/25.1.35>
- Lubac, B., and Loisel, H. (2007). Variability of classification of remote sensing reflectance spectra in the eastern English Channel and southern North Sea. *Remote Sens. Environ.*, 110, 45-58. <http://dx.doi.org/10.1016/j.rse.2007.02.012>
- Ma, R., Tang, J., Dai, J., Zhang, Y., and Song, Q. (2006). Absorption and scattering properties of water body in Taihu Lake, China: absorption. *Int. J. Remote Sens.*, 27(19), 4277-4304. <http://dx.doi.org/10.1080/01431160600851835>
- Metsamaa, L., Kutser, T., and Strombeck, N. (2006). Recognizing cyanobacterial blooms based on their optical signature. *Boreal Environ. Res.*, 11, 493-506.
- Miehle, P., Livesley, S.J., Liw, C., Feikemaz, P.M., Adams, M.A., and Arndt, S.K. (2006). Quantifying uncertainty from large-scale model predictions of forest carbon dynamics. *Global Change Biol.*, 12, 1421-1434. <http://dx.doi.org/10.1111/j.1365-2486.2006.01176.x>
- Mobley, C.D. (1999). Estimation of the remote-sensing reflectance from above-surface measurements. *Appl. Optics*, 38, 7442-7455. <http://dx.doi.org/10.1364/AO.38.007442>
- Morel, A., and Gentili, B. (1993). Diffuse reflectance of oceanic waters II: bidirectional aspects. *Appl. Optics*, 32, 6864-6879. <http://dx.doi.org/10.1364/AO.32.006864>
- Myint, S.W., and Walker, N.D. (2002). Quantification of surface suspended sediments along a river dominated coast with NOAA and SeaWiFS measurements: Louisiana, USA. *Int. J. Remote Sens.*, 23(16), 3229-3249. <http://dx.doi.org/10.1080/01431160110104700>
- Nechad, B., Ruddick, K.G., and Park, Y. (2010). Calibration and validation of a generic multisensory algorithm for mapping of total suspended matter in turbid waters. *Remote Sens. Environ.*, 114, 854-866. <http://dx.doi.org/10.1016/j.rse.2009.11.022>
- Odermatt, D., Gitelson, A., Brando, V.E., and Schaepman, M. (2012). Review of constituent retrieval in optically deep and complex waters from satellite imagery. *Remote Sens. Environ.*, 118, 116-126. <http://dx.doi.org/10.1016/j.rse.2011.11.013>
- Ohde, T., and Siegel, H. (2003). Derivation of immersion factors for the hyperspectral Trios radiance sensor. *J. Optics. A, Pure Appl. Optics*, 5(3), 12-14. <http://dx.doi.org/10.1088/1464-4258/5/3/103>
- Paerl, H., and Paul, V.J. (2012). Climate change: Links to global expansion of harmful cyanobacteria. *Water Res.*, 46, 1349-1363. <http://dx.doi.org/10.1016/j.watres.2011.08.002>
- Panigrahi, S., Wikner, J., Panigrahy, R.C., Satapathy, K.K., and Acharya, B.C. (2009). Variability of nutrients and phytoplankton biomass in a shallow brackish water ecosystem (Chilika Lagoon, India). *Limnology*, 10, 73-85. <http://dx.doi.org/10.1007/s10201-009->

0262-z

- Petus, C., Chust, G., Gohin, F., Doxaran, D., Froidefon, J.M., and Sagarmínaga, Y. (2010). Estimating turbidity and total suspended matter in the Adour River plume (South Bay of Biscay) using MODIS 250 m imagery. *Cont. Shelf Res.*, 30, 379-392. <http://dx.doi.org/10.1016/j.csr.2009.12.007>
- Pu, R.L., and Gong, P. (2000). *Hyperspectral Remote Sensing and Its Application*. Higher Education Press, Beijing.
- Randolph, K., Wilson, J., Tedesco, L., Li, L., Pascual, D. L., and Soyeux, E. (2008). Hyperspectral remote sensing of cyanobacteria in turbid productive water using optically active pigments, chlorophyll a and phycocyanin. *Remote Sens. Environ.*, 112, 4009-4019. <http://dx.doi.org/10.1016/j.rse.2008.06.002>
- Ruddick, K.G., De Cauwer, V., Park, Y.J., and Moore, G. (2006). Seaborne measurements of near infrared water-leaving reflectance: The similarity spectrum for turbid waters. *Limnol. Oceanogr.*, 51, 1167-1179. <http://dx.doi.org/10.4319/lo.2006.51.2.1167>
- Rundquist, D.C., Han, L., Schalles, J.F., and Peake, J.S. (1996). Remote measurement of algal chlorophyll in surface waters: the case for the first derivative of reflectance near 690 nm. *Photogramm. Eng. Remote Sens.*, 62, 195-200.
- Song, K.S., Li, L., Wang, Z.M., Liu, D.W., Zhang, B., Xu, J.P., Du, J., Li, L.H., and Li, S. (2012). Retrieval of total suspended matter and chlorophyll-a using remote sensing data for drinking water resources. *Environ. Monit. Assess.*, 184(3), 1449-1470. <http://dx.doi.org/10.1007/s10661-011-2053-3>
- Song, K.S., Wang, Z.M., Blackwell, J., Zhang, B., and Zhang, Y. (2011). Water quality monitoring using Landsat Thematic Mapper data with empirical algorithms in Chagan Lake, China. *J. Appl. Remote Sens.*, 5. <http://dx.doi.org/10.1117/1.3559497>
- Stumpf, R.P., and Pennock, J.R. (1989). Calibration of a general optical equation for remote sensing of suspended sediments in a moderately turbid estuary. *J. Geophys. Res.*, 94, 14363-14371. <http://dx.doi.org/10.1029/JC094iC10p14363>
- Sváb, E., Tyler, A.N., Preston, T., Presing, M., and Balogh, K.V. (2005). Characterizing the spectral reflectance of algae in lake waters with high suspended sediment concentrations. *Int. J. Remote Sens.*, 26(5), 919-928. <http://dx.doi.org/10.1080/0143116042000274087>
- Williams, P.C. (2001). Implementation of near infrared technology. In *Near infrared technology in the agricultural and food industries*, P.C. Williams and K.H. Norris (Ed.), 145-171 (St Paul, Minnesota: American Association of Cereal Chemists).
- Xu, J.P., Zhang, B., Li, F., Song, K.S., Wang, Z.M., Liu, D.W., and Zhang, G.X. (2009). Retrieval of total suspended matters using field spectral data in Shitoukoumen Reservoir, China. *Chin Geogr. Sci.*, 19(1), 77-82. <http://dx.doi.org/10.1007/s11769-009-0077-1>
- Yang, W., Matsushit, B., Chen, J., and Fukushima, T. (2011). Estimating constituent concentrations in case II waters from MERIS satellite data by semi-analytical model optimizing and look-up tables. *Remote Sens. Environ.*, 115, 1247-1259. <http://dx.doi.org/10.1016/j.rse.2011.01.007>